Journal Pre-proofs

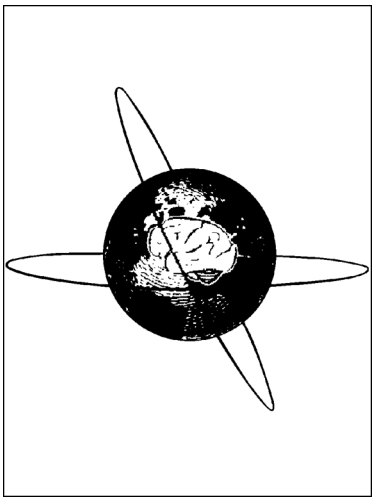

MEG Detection of High Frequency Oscillations and Intracranial-EEG Validation in Pediatric Epilepsy Surgery

Elaine Foley, Lucia R. Quitadamo, A. Richard Walsh, Peter Bill, Arjan Hillebrand, Stefano Seri

PII: S1388-2457(21)00615-5
DOI: https://doi.org/10.1016/j.clinph.2021.06.005
Reference: CLINPH 2009663

To appear in: *Clinical Neurophysiology*

Received Date: 18 September 2020
Revised Date: 23 May 2021
Accepted Date: 15 June 2021

Please cite this article as: Foley, E., Quitadamo, L.R., Richard Walsh, A., Bill, P., Hillebrand, A., Seri, S., MEG Detection of High Frequency Oscillations and Intracranial-EEG Validation in Pediatric Epilepsy Surgery, *Clinical Neurophysiology* (2021), doi: https://doi.org/10.1016/j.clinph.2021.06.005

MEG Detection of High Frequency Oscillations and Intracranial-EEG Validation in Pediatric Epilepsy Surgery

Elaine Foley[1], Lucia R. Quitadamo[1], A. Richard Walsh[2], Peter Bill[2], Arjan Hillebrand[3], Stefano Seri[1,2]

[1]Aston Institute of Health and Neurodevelopment, College of Health and Life Sciences, Aston University, Birmingham, UK

[2] Children's Epilepsy Surgery Program, The Birmingham Women's and Children's NHS Foundation Trust, Birmingham, UK

[3] Amsterdam UMC, Vrije Universiteit Amsterdam, Department of Clinical Neurophysiology and MEG Center, Amsterdam Neuroscience, De Boelelaan 1117, Amsterdam, The Netherlands

Corresponding Author:
Dr Elaine Foley
Aston Institute of Health and Neurodevelopment, College of Health and Life Sciences, Aston University, Aston Triangle, Birmingham, B4 7ET, UK
Tel: +44 (0121) 204 4755
Email: e.foley@aston.ac.uk

Highlights

1. High frequency oscillations (HFOs) can be automatically detected in non-invasive MEG recordings from paediatric epilepsy patients.

2. Sources of epileptic HFOs detected with MEG correspond well with sources of HFOs identified invasively from intracranial EEG recordings.

3. Concordance of MEG HFO sources with seizure onset zone//resected area demonstrates potential to aid surgical planning in paediatric epilepsy.

Abstract

Objective: To assess the feasibility of automatically detecting high frequency oscillations (HFOs) in magnetoencephalography (MEG) recordings in a group of ten paediatric epilepsy surgery patients who had undergone intracranial electroencephalography (iEEG).

Methods: A beamforming source-analysis method was used to construct virtual sensors and an automatic algorithm was applied to detect HFOs (80-250Hz). We evaluated the concordance of MEG findings with the sources of iEEG HFOs, the clinically defined seizure onset zone (SOZ), the location of resected brain structures, and with post-operative outcome.

Results: In 8/9 patients there was good concordance between the sources of MEG HFOs and iEEG HFOs and the SOZ. Significantly more HFOs were detected in iEEG relative to MEG $t(71)=2.85$, $p<.05$. There was good concordance between sources of MEG HFOs and the resected area in patients with good and poor outcome, however HFOs were also detected outside of the resected area in patients with poor outcome.

Conclusion: Our findings demonstrate the feasibility of automatically detecting HFOs non-invasively in MEG recordings in paediatric patients, and confirm compatibility of results with invasive recordings.

Significance: This approach provides support for the non-invasive detection of HFOs to aid surgical planning and potentially reduce the need for invasive monitoring, which is pertinent to paediatric patients.

Keywords:

MEG, Epilepsy, HFOs, Kurtosis, Paediatric age, iEEG, Automatic detection, Beamforming.

1. Introduction

Children and adolescents with refractory epilepsy are at increased risk of having long-term cognitive deficits and poor quality of life (Berg et al., 2004). Resective surgery is a therapeutic option for uncontrolled paediatric epilepsy that is gaining increasing acceptance (Cross et al., 2006). A recent randomized controlled trial has shown that seizure outcome following epilepsy surgery was significantly better than for continued medical treatment in paediatric surgical candidates (Dwivedi et al., 2017). Surgical outcome depends on a range of factors including, age, duration of epilepsy, type and lobe of surgery, and type of pathology (Blumcke et al., 2017; Ryvlin et al., 2014). Notably, an accurate delineation of the epileptogenic zone (EZ) is essential to achieve a positive surgical outcome. The EZ is defined as the area of cortex that is necessary and sufficient for initiating seizures and whose removal (or disconnection) is necessary for complete abolition of seizures (Rosenow and Luders, 2001). However, accurate identification of the EZ is challenging as there is no single diagnostic technique capable of directly measuring the EZ. This region is therefore assessed indirectly on the basis of multiple complementary diagnostic techniques, resulting in a set of specific zones built upon observable parameters (Rosenow and Luders, 2001). The Seizure Onset Zone (SOZ) is often used as a surrogate of the EZ in clinical practice, but a conclusive marker (structural or functional) to precisely delineate the SOZ, which could optimize pre-surgical evaluation and improve post-surgical outcome, is still lacking (Pitkänen et al., 2016).

High frequency oscillations (HFOs) in intracranial electroencephalography (iEEG) have been identified as potential biomarkers of epileptogenesis in recent years (Zijlmans et al., 2012). HFOs are electrophysiological transients occurring at frequencies above 80 Hz, and can be classified as ripples (80–250Hz) and fast ripples (250–500Hz). HFOs can be described as transient (burst-like) or continuous (steady-state), they can occur simultaneous with interictal epileptiform discharges (IEDs) or independently, and they have shown good spatial overlap with the SOZ in patients with focal epilepsy (Jacobs et al., 2008; Zijlmans et al., 2012). Retrospective studies in adults and children have found that resection of brain tissue that generates HFOs at high rates, leads to good post-surgical outcome (Fujiwara et al., 2012; Gallentine and Mikati, 2009; Jacobs et al., 2010; Usui et al., 2011). It has also been found that sources of fast ripples that were not resected during epilepsy surgery were linked to a poor surgical outcome (Weiss et al., 2018). Furthermore, a recent prospective study reported

that HFOs reliably predicted post-surgical outcome at the group level, and in two-thirds of patients at the individual level (Jacobs et al., 2018). While the results from invasive recordings are promising, the ultimate goal is to find a sensitive biomarker of epileptogenicity that can be recorded non-invasively, thereby reducing the need for invasive examinations in patients.

HFOs have been less frequently investigated non-invasively, yet recent studies have demonstrated that epileptic HFOs can be reliably detected using non-invasive methods such as scalp electroencephalography (EEG) (Andrade-Valenca et al., 2011; Kobayashi et al., 2010; Melani et al., 2013; Pizzo et al., 2016; van Klink et al., 2018; Zelmann et al., 2012) and magnetoencephalography (MEG) (Papadelis et al., 2016; van Klink et al., 2015; van Klink et al., 2017; Velmurugan et al., 2019, 2018; von Ellenrieder et al., 2016). Compared to iEEG, MEG non-invasively records whole-brain activity, offering better spatial sampling. In general, whole-head MEG systems also provide superior spatial resolution over clinical scalp EEG, making MEG a promising recording technique for HFO detection. However, whole-head MEG recordings produce a vast amount of data to be reviewed, making visual analysis of MEG HFO data extremely time consuming. More recently, automated HFO detectors have been developed with the aim of reducing reliance on visual detection and increasing reliability (Migliorelli et al., 2017; Quitadamo et al., 2018; van Klink et al., 2017).

A recent MEG study used a beamformer approach to create so-called virtual sensors, i.e. reconstructions of neuronal time-series in source-space, which have an increased signal to noise ratio compared to the sensor-level time-series. An automatic detection algorithm was then applied to successfully identify HFOs in the ripple band (van Klink et al., 2017). It has been shown that the HFO detection rate significantly increases in the virtual sensors compared to the physical sensors (van Klink et al., 2015). Thus, by combining methods such as beamforming with automated HFO detection algorithms it is possible to detect interictal HFOs with high sensitivity in MEG recordings (Thomschewski et al., 2019; van Klink et al., 2017; von Ellenrieder et al., 2016). Also, in a large sample (n=67) of patients with drug-resistant focal epilepsy HFOs found in ictal MEG recordings were concordant with the SOZ as identified with other modalities. Notably, resective surgery of the identified SOZ performed in six patients led to seizure freedom in all of them (Velmurugan et al., 2018).

Despite these promising results, recent reviews have concluded that evidence for the effective use of HFOs in epilepsy surgery decision-making is limited and further research is required (Gloss et al., 2017; Höller et al., 2015). Furthermore, the majority of previous studies have included patients with a broad age range, even though it has been recommended that a distinction should be made between analysis of HFOs in children and adults (Höller et al., 2015). The present study will therefore focus on HFO data from a group of paediatric patients only.

The aim of the present study was to assess the feasibility of automatically detecting HFOs in MEG recordings in the ripple frequency band (80–250Hz) in a group of ten paediatric patients with refractory epilepsy who were evaluated for epilepsy surgery. In order to gain a better understanding of the relationship between non-invasive and invasive HFOs, we aimed to directly compare non-invasive MEG data with iEEG recordings using a software tool developed by our group (Quitadamo et al., 2018b). For validation, we evaluated the concordance of our findings with the clinically defined SOZ, the three-dimensional (3D) location of resected brain structures, and with post-operative outcome at one year follow-up.

2. Methods

2.1 Participants

Ten pediatric patients (5 male; mean age = 13 years; SD= 3.6) with drug-resistant epilepsy under evaluation for resective surgery participated in the study. Patient demographics are summarized in Table 1. All patients were referred from Birmingham Women's and Children's Hospital NHS Foundation Trust to the Wellcome Laboratory for MEG studies at the Aston Brain Centre in Birmingham for localization of the irritative zone (the area of the brain that generates IEDs) and eloquent cortex mapping between 2015 and 2017. Postsurgical outcome according to the Engel classification (Durnford et al., 2011) was determined at one year follow up. This study was authorized by the R&D Department of the Birmingham Children's Hospital NHS Foundation Trust; as this study involved retrospective/secondary analysis of anonymised data obtained in the context of standard clinical practice retrospective consent was not required.

2.2 MEG Data Acquisition

MEG data were recorded in a magnetically shielded room using an Elekta-Neuromag TRIUX whole-head system (Helsinki, Finland) with 204 planar dc-SQUID gradiometers and 102 magnetometers. Participants were seated in the MEG scanner. Approximately 60 minutes of resting-state interictal data were acquired for each patient. Data were acquired with 2 KHz sampling rate, and low-pass filter of 660Hz. Data were acquired in 5 minute epochs to facilitate efficient computational analysis. One bipolar EEG channel was used to record the electrocardiogram (ECG). Five electromagnetic coils were positioned on the patient's head, three on the front and one on each mastoid to monitor head position. A Polhemus Fastrak device was used to digitize three fiducial points (nasion, left and right pre-auricular points), the electromagnetic head coils and the scalp surface, to facilitate translation between the MEG coordinate system and the patient's structural magnetic resonance image (MRI). Each participant's digitized scalp surface was co-registered with the scalp surface as extracted from a high-resolution anatomical MRI sequence.

2.3 MEG/MRI Co-registration

High-resolution anatomical MRI scans (3D inversion recovery whole-head volume sequences with $1mm^3$ isotropic resolution), were used for co-registration with the MEG data. Co-registration was performed using in-house surface matching software, to align the Polhemus and the MRI surfaces. The accuracy of this algorithm is within the order of a few mm (Adjamian et al., 2004; Whalen et al., 2008). Realistic, single-shell brain models were constructed for each participant based on their structural MRI (Nolte, 2003). Each patient's co-registered MRI was spatially normalized to a template MRI using the new segmentation toolbox in SPM8 in the MatlabR2012a environment (The MathWorks Inc., Natick, MA). 90 cortical and subcortical regions of interest (ROIs) were defined for further analysis using the automated anatomical labeling atlas (AAL) (Tzourio-Mazoyer et al., 2002), after inverse transformation to the patient's co-registered MRI (Hillebrand et al.,2012).

2.4 MEG Data Analysis

Preprocessing

MaxFilter software (Elekta Neuromag Oy, version 2.2.10) was used to remove artefacts from the raw data by implementing the temporal extension of signal space separation (tSSS) (Taulu and Simola, 2006). Bad channels were also identified and removed using MaxFilter, before applying tSSS. Each 5 minute dataset was then visually inspected for additional artefacts caused by muscle activity and SQUID jumps and any contaminated periods were removed.

HFO analysis

The data were filtered in the ripple band between 80-250 Hz using MaxFilter. A scalar beamformer implementation (Elekta Neuromag Oy, beamformer, version 2.2) similar to Synthetic Aperture Magnetometry (Robinson and Vrba, 1999) was used to reconstruct the time-series for the centroids of the 90 different cortical and subcortical ROIs. The centroid of an ROI was defined as the voxel within the ROI that is nearest (based on Euclidean distance) to all other voxels in that ROI (Hillebrand et al., 2016). The beamformer reconstructs the activity for each ROI sequentially by selectively weighting the contribution from each MEG sensor to an ROI's time-series. For the construction of the beamformer weights, the 80 Hz high-pass-filtered, pre-processed signal was used for data covariance, a unity matrix was used for the noise covariance and an equivalent dipole as the source model. Normalized beamformer weights were used to reconstruct the virtual sensor time-series (Cheyne et al., 2007; Hillebrand et al., 2005). The optimum dipole orientation was determined using Singular Value Decomposition (Sekihara et al., 2001). The ripple band (80-250 Hz) time-series were subsequently extracted from the 90 locations and used for further analysis.

IED analysis

The sensor time series data between 1-70 Hz were inspected for epileptiform spikes, and source localization was performed using an equivalent current dipole fitting approach in line with ACMEGS guidelines (Bagic et al., 2011). A single sphere head model based on the coregistered MRI scalp surface for each patient was used. A single moving equivalent current dipole (ECD) model was calculated at every sample from half-way up the rising phase of the spike to the peak, using the Elekta Source Modeling software Xfit (version 5.5.18). The source locations of the IEDs were used to compare with the sources of the HFOs for each patient.

2.5 Intracranial Data Acquisition and Preprocessing

Intracranial stereo-EEG (SEEG) recordings were acquired from 128 contacts in five patients using a commercial video-EEG monitoring system (System Plus, Micromed, Italy). The implantation sites and number of electrodes were determined based on clinical and anatomical data that were obtained during the non-invasive stage of the assessment. The number of contacts ranged between 5 - 18 per intracranial electrode, with a maximum of 192 recording channels. Data were sampled at 2 kHz and acquired with a band-pass filter of 0.016–1 kHz. Every channel was re-referenced off-line with respect to its nearest neighbor (bipolar derivations with 3.5 mm spatial resolution) to cancel-out the effects of volume conduction. Where appropriate for diagnostic purposes, the SEEG signal was referenced to the average signal from two electrodes identified to be in white matter, from anatomical and neurophysiological data. In addition to SEEG, two scalp EEG channels (Fz and Cz referenced to a mastoid electrode) and chin electromyogram were recorded for sleep staging. The duration of simultaneous video-SEEG recordings was between 5 and 10 days.

Intracranial strips or grids were implanted in five patients, where Platinum-iridium alloy electrode disks (Ad-Tech Medical Racine, WI, United States), of 4 mm diameter were arranged in a grid (max 8 × 8 array), a strip (4 × 1 or 6 × 1), and/or a combination of the two. Craniotomies and/or burr hole craniotomies were used to place electrodes in the subdural space as appropriate.

IEEG recordings were reviewed by an expert neurophysiologist, who marked the beginning of the seizures. The SOZ was anatomically defined by all of the contacts involved in seizure onset. Segments of iEEG data beginning 10 min before and lasting 2 min after the electrographic onset of each seizure were extracted. These were defined as the periods of interest for the identification of HFOs. Data were resampled to 1024 Hz (linear interpolation) and then visually inspected to identify artefactual channels, which were subsequently excluded.

2.6 HFO detection algorithm and HFO area determination

The algorithm for the detection of HFOs was applied in the same way for the analysis of both the MEG and iEEG data. The algorithm is described in depth in all its theoretical aspects and implementation details in Quitadamo et al., (2018a) and released within a software framework called EPINETLAB (Quitadamo et al., 2018b). Here we briefly report its main details.

The first step involves a procedure for the reduction of the number of channels/sources, based on their kurtotic value: for each channel, a wavelet-based time-frequency transform (e.g. Morlet) was computed on 1s windows and then the relative scalograms, representing the energy content of each wavelet coefficient, was determined. The spectral kurtosis, which usually achieves its peak where transient activities are present, was computed on each scalogram and its average values computed. Then the distribution of average kurtosis value was fitted against a set of standard statistical distributions that are available in the Matlab "Statistics and Machine Learning Toolbox" (e.g., normal, exponential, gamma, generalized extreme value, etc.). The one ranked first in terms of logarithmic likelihood was chosen as the one representative of the signal under analysis. The mean and the standard deviation (SD) values of the distribution were computed and a threshold set on the mean +3 SD. This threshold allows the discrimination of the most deviant kurtosis values on the right tail of the distribution. Channels were subsequently ranked based on the total number of windows with kurtosis values over the predefined threshold. After this ranking a subset of extremely kurtotic channels were retained for subsequent analysis.

The detection of HFOs was done by detecting as candidate HFOs those events where power exceeded the average power (over the entire 1s window) by 5 SD and for longer than 20 ms. Finally, events with power distributed over the whole frequency band or simultaneously present over many channels were discarded as artefact. Artefact rejection was initially performed automatically in MEG data and then further visual inspection was used. After HFOs have been detected on all the channels, it's important to define, on the basis of the channel HFO rates, which channels belong to the SOZ with the highest probability, the so called HFO area (see Quitadamo et al., 2018a for more details). HFO rates are expressed in terms of percentages, which represent the number of HFOs identified on a specific channel over the total number of HFOs detected. Sensitivity and specificity were calculated based on the iEEG data using the following criterion: true positives (TP) were defined as the channels corresponding to electrode contacts located in the HFO area and in the SOZ; false positives

(FP) were defined as channels located within the HFO area but not in the SOZ; true negatives (TN) were defined as the channels outside the HFO area and outside the SOZ and false negatives (FN) were channels located outside the HFO area but inside the SOZ. The sensitivity of the detection algorithm was defined as Sens = TP/(TP + FN) and the specificity as Spec = TN/(FP+TN), expressed in percentages. A binomial distribution was used to estimate confidence intervals.

The performance of this detection algorithm has been assessed previously on a sample of iEEG data comprising a combination of grid/strips and SEEG, that were acquired during presurgical evaluation of patients with drug-resistant epilepsy. The spatial concordance was assessed between the iEEG electrodes with the highest HFO (80-250 Hz) rates and the SOZ, which was determined using ictal and interictal iEEG as per standard clinical protocols (Quitadamo et al., 2018a,b). The results demonstrated good concordance between the sources of electrodes with the highest contribution of HFOs and the SOZ. The HFO findings were also supported by the 1-year post-surgical outcome.

2.7 Validation of MEG HFOs

The sources of the MEG HFOs (80-250 Hz) were visualized on the postoperative MRI of each of the patients to measure concordance with the resected area. Using similar criterion as used in a previous MEG study (van Klink et al., 2017), concordance was considered good if > 50% of the HFO sources were included in the resection, at lobar level, moderate if < 50% of HFO sources were included in the resection, and poor for discordance. Sources of the MEG HFOs were also compared to the locations of HFOs identified by iEEG, and to the clinically defined SOZ. The concordance between the MEG HFO sources and iEEG HFOs was assessed visually, using 3D slicer (Fedorov et al., 2012) and the same criterion as above was used i.e. concordance was considered good if > 50% of MEG HFO sources were identified in the same lobe as the iEEG HFOs and SOZ, moderate if < 50% of MEG HFO sources were identified in the same lobe as the iEEG HFOs and SOZ, and poor for discordance. A one-sample t-test was used to assess the difference between percentage HFO rate in the iEEG and MEG data.

Finally in those patients where IEDs were identified, concordance between source locations of HFOs and IEDs was also assessed at the lobar level using the same criterion as described

above. Post-operative outcome at 1 year follow up was used as a measure of overall success of the HFO detection process, as this is currently the clinical gold standard.

3. Results

3.1 Patients

Only those patients who had both MEG and intracranial monitoring as part of their presurgical evaluation at Birmingham Children's Hospital between 2015 and 2017 were included in the study. Ten patients met this inclusion criteria.

3.2 iEEG HFO detection

HFOs in the ripple band were reliably detected in the intracranial EEG of all 10 patients. The sources of these HFOs were compared to the SOZ, which was clinically defined by a neurophysiologist (PB) and epileptologist (SS). In the 10 patients, statistical comparison of the HFO areas with the clinically defined SOZ produced an overall mean sensitivity of 66% (SD 24%) and mean specificity of 92% (SD 5%; see Quitadamo et al., 2018a for full details of algorithm).

3.3 MEG HFO detection

MEG HFOs in the ripple band were detected in 9 out of 10 patients. HFOs were not detected in one patient's MEG data (case 4), but were detected in their iEEG data. Unfortunately the MEG data from this patient was extremely noisy due to excessive movement and EMG artefact. It was therefore not possible to get sufficient 'clean' segments of data for HFO detection. In addition, IEDs could not be detected in the MEG data for this patient either. This patient was therefore excluded from further analysis.

In the remaining 9 cases there was overall good concordance between HFO locations identified intracranially and extracranially. There was a significant difference between the percentage rate of HFOs detected in iEEG and MEG data $t(71) = 2.85$, $p < .05$. Significantly more HFOs were detected in the iEEG data (mean HFO rate = 13.75%, SD = 6.34) than in

the MEG data (mean HFO rate = 9.34%, SD = 6.64). In 8/9 patients there was good concordance between the sources of MEG HFOs and the iEEG HFOs and the SOZ (see Table 2 and Figure 1). In 6 of those patients MEG HFOs were identified within the SOZ and in the other 2 patients HFOs were detected in close proximity to the SOZ i.e. within the same lobe. Of these 8 patients, 5 had good outcome (Engel I /II) and 3 had poor outcome (Engel III/IV). IEDs were only present in the MEG data in 4 of these patients (cases 1,2,3,7) and were concordant with the source locations of HFOs and the SOZ (see Table 2).

In 7/9 patients there was good concordance with the resected area, in one patient there was moderate concordance and 1 patient was discordant (see Table 2). In terms of outcome, 4/6 patients with good outcome had concordant MEG HFOs with resected area, there was moderate concordance in 1 patient and 1 patient with good outcome was discordant. In 3/3 patients with poor outcome MEG HFOs were concordant with the resected area, although a proportion of HFOs (< 50%) were also detected outside of the resected area in all three of these patients (see Table 2). In the one discordant patient (case 7) MEG HFOs were detected in the hemisphere opposite to the SOZ and resected area. This patient was a particularly complicated case with bilateral frontal and temporal SEEG implantation. The patient had a left superior frontal gyrus resection bounded by somato-motor area (SMA). MEG HFOs were identified in the right frontal, parietal and temporal lobes. Interestingly HFOs in the iEEG data were detected in both left and right frontal contacts. So the MEG HFOs were partially concordant with the sources of the iEEG HFOs. In addition MEG IEDs were identified in bilateral temporal and right frontal lobes, which were also discordant with the SOZ. Nevertheless, despite being a complicated case, this patient had a good post-operative outcome (Engel IA)

4. Discussion

In this study, we applied a novel automatic method, recently developed by our group, for the detection of HFOs in MEG and iEEG data. We evaluated the topographic concordance between HFOs in the ripple frequency band (80-250 Hz) present in source-space MEG data and those identified in iEEG in ten paediatric patients with refractory epilepsy who had undergone presurgical evaluation. We also validated the MEG findings against the clinically defined SOZ, resected brain area and against post-operative outcome at 1 year follow-up.

After excluding one patient due to excessive artefacts in their MEG data, we found overall good concordance in nine patients between the sources of HFOs identified in the MEG and iEEG data. We found good concordance in eight patients between the sources of MEG HFOs and the SOZ: 5/6 patients with good outcome and 3/3 patients with poor outcome. Similarly we found good concordance in seven patients between sources of MEG HFOs and the resected area, in one patient there was moderate concordance and one patient was discordant. In the three patients with poor outcome MEG HFOs were overall concordant with the resection area, however in all three cases HFOs were also detected in areas outside of the resection cavity. Our findings demonstrate the feasibility of the automatic detection of HFOs in clinical non-invasive MEG recordings in a paediatric sample, and demonstrate the compatibility of results with invasive recordings in the same patients.

Despite converging evidence from animal and human studies on the potential role of HFOs as a biomarker for epileptogenicity, their application in clinical practice in epilepsy surgery decision-making is still limited (Gloss et al., 2017; Höller et al., 2015). This is presumably due to a number of factors, a contributing factor may be that up until recently the focus has largely been on invasive recordings. The development of a HFO biomarker based on non-invasive recordings would increase their clinical potential and reduce the requirement for long-term monitoring and invasive intracranial recordings. It was previously believed that the non-invasive detection of HFOs with MEG and EEG was not possible because the generators would be too weak to distinguish from background noise (von Ellenrieder etal., 2014). However, recent studies have shown that HFOs can be reliably detected non-invasively in both EEG and MEG recordings. A few studies have identified interictal HFOs in MEG as visible events in the time domain, as typically performed in iEEG (van Klink et al., 2015; von Ellenrieder et al., 2016), while the majority of MEG studies have focused on time-frequency analyses (Miao et al., 2014; Rampp et al., 2010; Tenney et al., 2014; Xiang et al., 2010). In particular, sources of MEG high frequency components identified in the ripple frequency band have been shown to be related to the EZ (van Klink et al., 2017). However, very few studies have directly compared HFOs detected non-invasively with MEG with those identified during iEEG recordings.

In a unique study, Rampp et al. (2010) simultaneously recorded MEG and iEEG in six adult patients during pre-surgical evaluation. They found that sources of spike-locked or spike independent high gamma oscillations (50-120 Hz) detected with MEG and iEEG were strongly associated with the SOZ. This study was one of the first to provide evidence that MEG high gamma oscillations corresponded directly to those recorded invasively with iEEG in adult patients. These findings are broadly consistent with the present study, although not acquired simultaneously, we applied the same analysis pipeline and algorithm to detect HFOs in MEG and iEEG recordings and found good concordance in all nine patients. Notably, we found that significantly higher rates of HFOs were detected with iEEG compared to MEG. This may reflect the better signal to noise ratio of iEEG recordings. It may also be related to the fact that the iEEG data segments were extracted from ictal recordings (although pre-ictal and post-ictal segments were analysed here), whereas the MEG data segments were all extracted from interictal recordings. Nevertheless, we have demonstrated that HFOs can be reliably detected both invasively and non-invasively. Papadelis et al. (2016) also found good concordance between sources of HFOs (80-150 Hz) detected in MEG and iEEG recordings in one paediatric patient. Unfortunately these previous studies are limited by the small sample sizes and also by the lack of post-surgical outcome data to validate their findings. In order to establish HFOs as non-invasive biomarkers, it is imperative to validate HFO source localization results against post-surgical outcome data, which is the current clinical gold standard.

We attempted to address this in the present study by relating our HFO findings to post-surgical outcome data. Interestingly, in 3/3 patients with poor outcome a proportion of HFOs were detected in sources outside of the resected area. For example, in case 3 who had a right insular/opercular superior termporal gyrus resection with poor outcome at 1 year follow-up (Engel IVB), the majority of MEG and iEEG HFOs were detected within the resected area, yet MEG HFOs were also detected in the parahippocampal gyrus which was not included in the resection. Case 6 had a left superior temporal gyrus resection with a poor outcome (Engel IIIC), while the majority of MEG HFOs were detected within the left temporal lobe an additional source of HFOs was identified in the left supramarginal gyrus. Case 9 had a left temporal lobectomy with hippocampectomy and also had a poor outcome (Engel IVB). In this case, MEG HFOs were detected in three sources in the left superior temporal gyrus and superior temporal pole, but also in the left mid orbitofrontal gyrus, which was not within the

area of resection. Given the poor outcome in these patients it implies that the area of resection did not fully cover the EZ. It has been shown that patients with additional sources of MEG HFOs (Velmurugan et al., 2019) and iEEG HFOs (van ’t Klooster et al., 2015) that were not surgically resected, were more likely to have poor outcome. We could therefore speculate in the present study that outcome may have improved if the additional HFO sources were included in the resected area.

Due to the relatively small sample size and the retrospective nature of our study it was not possible to predict post-surgical outcome from our data. However, a large prospective study (Velmurugan et al., 2019) recently investigated the clinical utility of MEG HFOs during pre-surgical examination and assessed their role in predicting post-surgical outcome in 52 predominantly adult patients (mean age 22.94 years) who were undergoing resective surgery for refractory epilepsy. Seizure outcomes could be predicted based on whether or not MEG HFO sources were included within the resection. The accuracy of localizing the resected cortex was 70% for HFO sources, compared to 59% for spike dipole analysis, which is the current clinical standard. Furthermore, patients had an 82.4% chance of seizure freedom when the location of HFO sources was included in the resection area. These results are in line with findings from studies of invasive HFOs (Andrade-Valenca et al., 2011; van ’t Klooster et al., 2015) and provide strong support for the application of non-invasive HFO recordings in routine pre-surgical evaluation. However, a couple of limitations regarding the methods must be addressed.

Firstly, typical HFO analysis is based on detecting spike-locked HFOs only, but previous MEG studies have found that around 30% of patients do not show epileptiform abnormalities at the time of recording (Rampp et al., 2019; van Klink et al., 2017). A method that is capable of detecting both spike-locked and spike-independent HFOs would be valuable in these cases (Rampp et al., 2019; van Klink et al., 2017). Notably, in the present study we had a relatively high proportion of patients (~50%) who did not display epileptiform abnormalities in their MEG data, yet HFOs were successfully detected in these patients. There are a number of reasons why spikes were not detected in these patients, including the relatively short MEG recording period (~1 hour) compared to invasive recordings, which are performed over days. Furthermore, there was no medication reduction prior to MEG recordings and all of the

patients were awake during recording. Our findings therefore highlight the added value of using a method that can detect spike-independent HFOs, as it can provide valuable non-invasive information on the location of the hypothesized EZ in those patients for whom interictal/ictal epileptiform activity is not present.

Secondly, in the study by Velmurugan and colleagues every spike epoch in every virtual sensor was visually evaluated, which is extremely time-consuming and may be impractical in clinical practice. Algorithms for the automatic detection of HFOs have been developed to address this issue and have been applied to both invasive and non-invasive recordings with varying success (Migliorelli et al., 2017; Navarrete et al., 2016; Quitadamo, et al., 2018; Shimamoto et al., 2018; van Klink et al., 2017). The novel aspect of the HFO detection algorithm applied in the present study is the use of a kurtosis-based metric to select a subset of channels that are most likely to be related to the SOZ, rather than relying on a priori knowledge of seizure onset location in the implanted electrodes. Kurtosis has previously been applied in clinical epilepsy studies for first-pass selection of virtual channels in beamformer-based analysis of MEG data (Hall et al., 2018; Robinson et al., 2004). The main advantage of using this kurtosis-based approach is to reduce computational complexity, by providing a metric for the selection of a subset of informative channels (Quitadamo et al., 2018a). This is essential when handling multichannel and long-term iEEG and MEG data with high sampling rates. Furthermore, the toolbox developed by our group provides a means of importing and analyzing MEG data, and comparing results of the SOZ with complementary methodologies such as iEEG (Quitadamo et al., 2018b).

This tool was initially validated on a group of patients who underwent iEEG investigations and were successfully operated on. The results revealed good concordance between electrodes with the highest contribution of HFOs in the ripple frequency band and the SOZ identified clinically. However, it must be noted that the tool was originally developed and tested in the ripple frequency band (80-250 Hz) only, due to sample rate constraints of the iEEG test dataset. It is for this reason that we also focused our MEG analysis on the ripple band in the present study. We also focused on the 80-250 Hz range in an effort to reduce contamination from head position indicator (HPI) coils which were used for tracking head motion during the MEG recording. These coils are energized at frequencies between 293 and

328 Hz. While there is a growing body of literature on the contribution of fast ripple HFOs (250-500 Hz) to SOZ identification (Bernardo et al., 2018; Fedele et al., 2017) and reports have shown them to be highly correlated with positive surgical outcome in iEEG (van 't Klooster et al., 2017), there is currently little data on the non-invasive detection of fast ripples. Notably, a couple of studies have demonstrated that fast ripples can be detected in scalp EEG (Bernardo et al., 2018; Pizzo et al., 2016), but they have been described as more difficult to detect due to their smaller generators and the amplifier noise at frequencies above 200 Hz. It has also been suggested that fast ripples may be more feasible to detect in scalp EEG in paediatric populations where the skull is thinner, leading to decreased signal attenuation (Bernardo et al., 2018).

Determining a non-invasive biomarker is particularly important in paediatric drug-resistant epilepsy, as these children represent a vulnerable patient population due to the detrimental effects of uncontrolled seizures on neurodevelopment and cognition (Ibrahim et al., 2012). Advances in the surgical treatment of intractable epilepsy have contributed to improvements in seizure outcomes and also cognitive outcomes in paediatric patients (Braun, 2017; Braun and Cross, 2018). Interestingly, a recent study has reported that fast ripples in intra-operative electrocorticography could be potential predictive markers of post-surgical cognitive outcome in pediatric epilepsy surgery (Sun et al., 2020). The authors found that the removal of tissue generating HFOs (250-500 Hz) was associated with cognitive improvement in children following surgery beyond the benefits of seizure reduction, and suggest that surgical tailoring using HFOs rather than spikes may result in better cognitive outcome in children (Sun et al., 2020). This study highlights the value of using of HFOs to guide surgical resection, to not only improve surgical outcome in terms of seizure freedom but also with respect to cognitive outcomes. It would be interesting to establish if similar findings could be obtained non-invasively.

5. Conclusion

In conclusion, we have demonstrated the feasibility of automatically detecting HFOs in MEG recordings in the ripple frequency band (80–250Hz) in a group of paediatric patients with refractory epilepsy. Furthermore, we have shown good topographic concordance between HFOs present in source-space MEG data and those identified in iEEG data in the same group

of patients. We also found good concordance between the sources of MEG and iEEG HFOs, the SOZ and the resected area. We found overall good concordance between sources of HFOs and the area of resection in patients with good and poor post-surgical outcome. However we did find that patients with poor outcome had a proportion of HFOs that were detected outside of the resected area. Taken together these findings provide support for the clinical value of non-invasively detecting HFOs to aid surgical planning and potentially reduce the need for invasive monitoring, which is pertinent to paediatric patients. Furthermore, the current approach, which revealed spike-independent HFOs, may be particularly useful in patients who do not reveal interictal/ictal epileptiform activity in their MEG recordings.

Acknowledgements

This study has received funding from the European Union's Horizon 2020 research and innovation program under the Marie Sklodowska-Curie Grant agreement No. 655016.

Conflict of Interest

None of the authors have potential conflicts of interest to be disclosed.

References

Adjamian, P., Barnes, GR., Hillebrand, A., Holliday, IE., Singh, KD., Furlong, PL., et al. (2004). Co-registration of magnetoencephalography with magnetic resonance imaging using bite-bar-based fiducials and surface-matching. *Clin Neurophysiol*, *115*(3), 691–698. https://doi.org/10.1016/j.clinph.2003.10.023

Andrade-Valenca, LP., Dubeau, F., Mari, F., Zelmann, R., Gotman, J. (2011). Interictal scalp fast oscillations as a marker of the seizure onset zone. *Neurology*, *77*(6), 524 LP – 531. https://doi.org/10.1212/WNL.0b013e318228bee2

Berg, AT., Smith, SN., Frobish, D., Beckerman, B., Levy, SR., Testa, FM., Shinnar, S. (2004). Longitudinal assessment of adaptive behavior in infants and young children with newly diagnosed epilepsy: influences of etiology, syndrome, and seizure control. *Pediatrics*, *114*(3), 645–650. https://doi.org/10.1542/peds.2003-1151-L

Bernardo, D., Nariai, H., Hussain, SA., Sankar, R., Salamon, N., Krueger, DA., et al. (2018). Visual and semi-automatic non-invasive detection of interictal fast ripples: A potential biomarker of epilepsy in children with tuberous sclerosis complex. *Clin Neurophysiol*, *129*(7), 1458–1466. https://doi.org/https://doi.org/10.1016/j.clinph.2018.03.010

Blumcke, I., Spreafico, R., Haaker, G., Coras, R., Kobow, K., Bien, CG., et al. (2017). Histopathological Findings in Brain Tissue Obtained during Epilepsy Surgery. *N Engl J Med*, *377*(17), 1648–1656. https://doi.org/10.1056/NEJMoa1703784

Braun, KPJ. (2017). Preventing cognitive impairment in children with epilepsy. *Curr Opin Neurol*, *30*(2), 140–147. https://doi.org/10.1097/WCO.0000000000000424

Braun, KPJ, Cross, JH. (2018). Pediatric epilepsy surgery: the earlier the better. *Expert Rev Neurother 18(4), 261-263.* https://doi.org/10.1080/14737175.2018.1455503

Cheyne, D., Bostan, AC., Gaetz, W., Pang, EW. (2007). Event-related beamforming: A robust method for presurgical functional mapping using MEG. *Clin Neurophysiol*, *118*(8), 1691–1704. https://doi.org/https://doi.org/10.1016/j.clinph.2007.05.064

Cross, JH., Jayakar, P., Nordli, D., Delalande, O., Duchowny, M., Wieser, HG., et al. (2006). Proposed criteria for referral and evaluation of children for epilepsy surgery: Recommendations of the subcommission for pediatric epilepsy surgery. *Epilepsia*, *47*(6), 952–959. https://doi.org/10.1111/j.1528-1167.2006.00569.x

Durnford, AJ., Rodgers, W., Kirkham, FJ., Mullee, MA., Whitney, A., Prevett, M., et al. (2011). Very good inter-rater reliability of Engel and ILAE epilepsy surgery outcome classifications in a series of 76 patients. *Seizure*, *20*(10), 809–812. https://doi.org/10.1016/j.seizure.2011.08.004

Dwivedi, R., Ramanujam, B., Chandra, P. S., Sapra, S., Gulati, S., Kalaivani, M., et al. (2017). Surgery for drug-resistant epilepsy in children. *N Engl J Med*, *377*(17), 1639–1647. https://doi.org/10.1056/NEJMoa1615335

Fedele, T., Ramantani, G., Burnos, S., Hilfiker, P., Curio, G., Grunwald, T., et al. (2017). Prediction of seizure outcome improved by fast ripples detected in low-noise intraoperative corticogram. *Clin Neurophysiol*, *128*(7), 1220–1226. https://doi.org/https://doi.org/10.1016/j.clinph.2017.03.038

Fedorov, A., Beichel, R., Kalpathy-Cramer, J., Finet, J., Fillion-Robin, J.-C., Pujol, S.,et al.

(2012). 3D Slicer as an Image Computing Platform for the Quantitative Imaging Network. *Magn Reson Imaging*, *30*(9), 1323–1341. https://doi.org/10.1016/j.mri.2012.05.001.3D

Fujiwara, H., Greiner, HM., Lee, KH., Holland-Bouley, KD., Seo, JH., Arthur, T., et al. (2012). Resection of ictal high-frequency oscillations leads to favorable surgical outcome in pediatric epilepsy. *Epilepsia*, *53*(9), 1607–1617. https://doi.org/10.1111/j.1528-1167.2012.03629.x

Gallentine, WB., Mikati, MA. (2009). Intraoperative electrocorticography and cortical stimulation in children. *J Clin Neurophysiol*, *26*(2), 95–108. https://doi.org/10.1097/WNP.0b013e3181a0339d

Gloss, D., Nevitt, SJ., Staba, R. (2017). The role of high-frequency oscillations in epilepsy surgery planning. *Cochrane Database Syst Rev*, *2017*(10). https://doi.org/10.1002/14651858.CD010235.pub3

Hall, MBH., Nissen, IA., van Straaten, ECW., Furlong, PL., Witton, C., Foley, E., et al. (2018). An evaluation of kurtosis beamforming in magnetoencephalography to localize the epileptogenic zone in drug resistant epilepsy patients. *Clin Neurophysiol*, *129*(6), 1221–1229. https://doi.org/10.1016/j.clinph.2017.12.040

Hillebrand, A., Nissen, IA., Ris-Hilgersom, I., Sijsma, NCG., Ronner, HE., van Dijk, BW., et al. (2016). Detecting epileptiform activity from deeper brain regions in spatially filtered MEG data. *Clin Neurophysiol*, *127*(8), 2766–2769. https://doi.org/10.1016/j.clinph.2016.05.272

Hillebrand, A., Barnes, GR., Bosboom, JL., Berendse, HW., Stam, CJ. (2012). Frequency-dependent functional connectivity within resting-state networks: an atlas-based MEG beamformer solution. *NeuroImage*, *59*(4), 3909–3921. https://doi.org/10.1016/j.neuroimage.2011.11.005

Hillebrand, A, Singh, KD., Holliday, IE., Furlong, PL., Barnes, GR. (2005). A new approach to neuroimaging with magnetoencephalography. *Hum Brain Mapp*, *25*(2), 199–211. https://doi.org/10.1002/hbm.20102

Höller, Y., Kutil, R., Klaffenböck, L., Thomschewski, A., Höller, PM., Bathke, AC., et al. (2015). High-frequency oscillations in epilepsy and surgical outcome. A meta-analysis. *Front Hum Neurosci*, 9, 1–14. https://doi.org/10.3389/fnhum.2015.00574

Ibrahim, GM., Fallah, A., Snead, OC., Drake, JM., Rutka, JT., Bernstein, M. (2012). The use of high frequency oscillations to guide neocortical resections in children with medically-intractable epilepsy: How do we ethically apply surgical innovations to patient care? *Seizure*, *21*(10), 743–747. https://doi.org/10.1016/j.seizure.2012.07.013

Jacobs, J., LeVan, P., Chander, R., Hall, J., Dubeau, F., Gotman, J. (2008). Interictal high-frequency oscillations (80-500 Hz) are an indicator of seizure onset areas independent of spikes in the human epileptic brain. *Epilepsia*, *49*(11), 1893–1907. https://doi.org/10.1111/j.1528-1167.2008.01656.x

Jacobs, J., Wu, JY., Perucca, P., Zelmann, R., Mader, M., Dubeau, F., et al. (2018). Removing high-frequency oscillations: A prospective multicenter study on seizure outcome. *Neurology*, *91*(11), e1040–e1052. https://doi.org/10.1212/WNL.0000000000006158

Jacobs, J., Zijlmans, M., Zelmann, R., Chatillon, CÉ., Hall, J., Olivier, A., et al. (2010). High-frequency electroencephalographic oscillations correlate with outcome of epilepsy surgery. *Ann Neurol*, *67*(2), 209–220. https://doi.org/10.1002/ana.21847

Kobayashi, K., Agari, T., Oka, M., Yoshinaga, H., Date, I., Ohtsuka, Y., Gotman, J. (2010). Detection of seizure-associated high-frequency oscillations above 500Hz. *Epilepsy Res*, *88*(2–3), 139–144. https://doi.org/10.1016/j.eplepsyres.2009.10.008

Melani, F., Zelmann, R., Dubeau, F., Gotman, J. (2013). Occurrence of scalp-fast oscillations among patients with different spiking rate and their role as epileptogenicity marker. *Epilepsy Res*, *106*(3), 345–356. https://doi.org/https://doi.org/10.1016/j.eplepsyres.2013.06.003

Miao, A., Xiang, J., Tang, L., Ge, H., Liu, H., Wu, T., et al. (2014). Using ictal high-frequency oscillations (80-500Hz) to localize seizure onset zones in childhood absence epilepsy: A MEG study. *Neurosci Lett*, *566*, 21–26. https://doi.org/10.1016/j.neulet.2014.02.038

Migliorelli, C., Alonso, JF., Romero, S., Nowak, R., Russi, A., Mañanas, MA. (2017). Automated detection of epileptic ripples in MEG using beamformer-based virtual sensors. *J Neural Eng*, *14*(4). https://doi.org/10.1088/1741-2552/aa684c

Navarrete, M., Pyrzowski, J., Corlier, J., Valderrama, M., Le Van Quyen, M. (2016). Automated detection of high-frequency oscillations in electrophysiological signals: Methodological advances. *J Physiol (Paris)*, *110*(4), 316–326. https://doi.org/https://doi.org/10.1016/j.jphysparis.2017.02.003

Nolte, G., 2003. The magnetic lead field theorem in the quasi-static approximation and its use for magnetoencephalography forward calculation in realistic volume conductors. Phys Med Biol 48, 3637–3652. https://doi.org/10.1088/0031-9155/48/22/002.

Papadelis, C., Tamilia, E., Stufflebeam, S., Grant, PE., Madsen, JR., Pearl, PL., Tanaka, N. (2016). Interictal High Frequency Oscillations Detected with Simultaneous Magnetoencephalography and Electroencephalography as Biomarker of Pediatric Epilepsy. *J Vis Exp*, (118), 1–13. https://doi.org/10.3791/54883

Pitkänen, A., Löscher, W., Vezzani, A., Becker, AJ., Simonato, M., Lukasiuk, K., et al. (2016). Advances in the development of biomarkers for epilepsy. *Lancet Neurol*, *15*(8), 843–856. https://doi.org/10.1016/S1474-4422(16)00112-5

Pizzo, F., Frauscher, B., Ferrari-Marinho, T., Amiri, M., Dubeau, F., Gotman, J. (2016). Detectability of Fast Ripples (>250 Hz) on the Scalp EEG: A Proof-of-Principle Study with Subdermal Electrodes. *Brain Top*, *29*(3), 358–367. https://doi.org/10.1007/s10548-016-0481-7

Quitadamo, LR., Foley, E., Mai, R., de Palma, L., Specchio, N., Seri, S. (2018). EPINETLAB: A Software for Seizure-Onset Zone Identification From Intracranial EEG Signal in Epilepsy. *Front Neuroinform*, *12*(July), 1–15. https://doi.org/10.3389/fninf.2018.00045

Quitadamo, LR., Mai, R., Gozzo, F., Pelliccia, V., Cardinale, F., Seri, S. (2018). Kurtosis-Based Detection of Intracranial High-Frequency Oscillations for the Identification of the Seizure Onset Zone. *Int J Neural Syst*, *28*(7), 1–18. https://doi.org/10.1142/S0129065718500016

Rampp, S., Kaltenhäuser, M., Weigel, D., Buchfelder, M., Blümcke, I., Dörfler, A., Stefan, H. (2010). MEG correlates of epileptic high gamma oscillations in invasive EEG. *Epilepsia*, *51*(8), 1638–1642. https://doi.org/10.1111/j.1528-1167.2010.02579.x

Rampp, S., Stefan, H., Wu, X., Kaltenhäuser, M., Maess, B., Schmitt, F. C., et al. (2019). Magnetoencephalography for epileptic focus localization in a series of 1000 cases. *Brain*, *142*(10), 3059–3071. https://doi.org/10.1093/brain/awz231

Robinson, SE., Nagarajan, SS., Mantle, M., Gibbons, V., Kirsch, H. (2004). Localization of interictal spikes using SAM(g2) and dipole fit. *Neurol Clin Neurophysiol*, *2004*, 1–7.

Robinson, S., Vrba, J. (1999). Functional neuroimaging by synthetic aperture magnetometry (SAM). In *Recent advances in biomagnetism* (pp. 302–305). Sendai: Tohoku University Press.

Rosenow, F., Luders, H. (2001). Presurgical evaluation of epilepsy. *Brain*, *124*, 1683–1700. https://doi.org/doi: 10.1093/brain/124.9.1683

Ryvlin, P., Cross, J. H., Rheims, S. (2014). Epilepsy surgery in children and adults. *Lancet Neurol*, *13*(11), 1114–1126. https://doi.org/10.1016/S1474-4422(14)70156-5

Sekihara, K., Nagarajan, SS., Poeppel, D., Marantz, A., Miyashita, Y. (2001). Reconstructing spatio-temporal activities of neural sources using an MEG vector beamformer technique. *IEEE T Bio-Med Eng*, *48*(7), 760–771. https://doi.org/10.1109/10.930901

Shimamoto, S., Waldman, ZJ., Orosz, I., Song, I., Bragin, A., Fried, I., et al. (2018). Utilization of independent component analysis for accurate pathological ripple detection in intracranial EEG recordings recorded extra- and intra-operatively. *Clin Neurophysiol*, *129*(1), 296–307. https://doi.org/https://doi.org/10.1016/j.clinph.2017.08.036

Sun, D., van 't Klooster, MA., van Schooneveld, MMJ., Zweiphenning, WJEM., van Klink, NEC., Ferrier, CH., et al. (2020). High frequency oscillations relate to cognitive improvement after epilepsy surgery in children. *Clin Neurophysiol*, *131*(5), 1134–1141. https://doi.org/10.1016/j.clinph.2020.01.019

Taulu, S., Simola, J. (2006). Spatiotemporal signal space separation method for rejecting nearby interference in MEG measurements. *Phys Med Biol*, *51*(7), 1759–1768. https://doi.org/10.1088/0031-9155/51/7/008

Tenney, JR., Fujiwara, H., Horn, PS., Vannest, J., Xiang, J., Glauser, TA., Rose, DF. (2014). Low- and high-frequency oscillations reveal distinct absence seizure networks. *Ann Neurol*, *76*(4), 558–567. https://doi.org/10.1002/ana.24231

Thomschewski, A., Hincapié, AS., Frauscher, B. (2019). Localization of the epileptogenic zone using high frequency oscillations. *Front Neurol*, *10*(94), 1-19. https://doi.org/10.3389/fneur.2019.00094

Tzourio-Mazoyer, N., Landeau, B., Papathanassiou, D., Crivello, F., Etard, O., Delcroix, N., et al. (2002). Automated anatomical labeling of activations in SPM using a macroscopic anatomical parcellation of the MNI MRI single-subject brain. *NeuroImage*, *15*(1), 273–289. https://doi.org/10.1006/nimg.2001.0978

Usui, N., Terada, K., Baba, K., Matsuda, K., Nakamura, F., Usui, K., et al. (2011). Clinical significance of ictal high frequency oscillations in medial temporal lobe epilepsy. *Clin Neurophysiol*, *122*(9), 1693–1700.

https://doi.org/https://doi.org/10.1016/j.clinph.2011.02.006

van 't Klooster, MA., van Klink, NEC., Leijten, FSS., Zelmann, R., Gebbink, TA., Gosselaar, PH., et al. (2015). Residual fast ripples in the intraoperative corticogram predict epilepsy surgery outcome. *Neurology*, *85*(2), 120–128. https://doi.org/10.1212/WNL.0000000000001727

van 't Klooster, MA., van Klink, NEC., Zweiphenning, WJEM., Leijten, FSS., Zelmann, R., Ferrier, CH., et al. (2017). Tailoring epilepsy surgery with fast ripples in the intraoperative electrocorticogram. *Ann Neurol*, *81*(5), 664–676. https://doi.org/10.1002/ana.24928

van Klink, N., Hillebrand, A., Zijlmans, M. (2015). Identification of epileptic high frequency oscillations in the time domain by using MEG beamformer-based virtual sensors. *Clin Neurophysiol*. https://doi.org/10.1016/j.clinph.2015.06.008

van Klink, N., Mol, A., Ferrier, C., Hillebrand, A., Huiskamp, G., Zijlmans, M. (2018). Beamforming applied to surface EEG improves ripple visibility. *Clin Neurophysiol*, *129*(1), 101–111. https://doi.org/https://doi.org/10.1016/j.clinph.2017.10.026

van Klink, N., van Rosmalen, F., Nenonen, J., Burnos, S., Helle, L., Taulu, S., et al. (2017). Automatic detection and visualisation of MEG ripple oscillations in epilepsy. *NeuroImage: Clinical*, *15*, 689–701. https://doi.org/10.1016/j.nicl.2017.06.024

Velmurugan, J., Nagarajan, SS., Mariyappa, N., Mundlamuri, RC., Raghavendra, K., Bharath, RD., et al. (2019). Magnetoencephalography imaging of high frequency oscillations strengthens presurgical localization and outcome prediction. *Brain*, 1–16. https://doi.org/10.1093/brain/awz284

Velmurugan, J., Nagarajan, SS., Mariyappa, N., Ravi, SG., Thennarasu, K., Mundlamuri, R. C., et al. (2018). Magnetoencephalographic imaging of ictal high-frequency oscillations (80-200 Hz) in pharmacologically resistant focal epilepsy. *Epilepsia*, *59*(1), 190–202. https://doi.org/10.1111/epi.13940

von Ellenrieder, N., Beltrachini, L., Muravchik, CH., Gotman, J. (2014). Extent of cortical generators visible on the scalp: Effect of a subdural grid. *NeuroImage*, *101*, 787–795. https://doi.org/10.1016/j.neuroimage.2014.08.009

von Ellenrieder, N., Pellegrino, G., Hedrich, T., Gotman, J., Lina, JM., Grova, C., Kobayashi, E. (2016). Detection and Magnetic Source Imaging of Fast Oscillations (40–160 Hz) Recorded with Magnetoencephalography in Focal Epilepsy Patients. *Brain Top*, *29*(2), 218–231. https://doi.org/10.1007/s10548-016-0471-9

Weiss, S. A., Berry, B., Chervoneva, I., Waldman, Z., Guba, J., Bower, M., et al. (2018). Visually validated semi-automatic high-frequency oscillation detection aides the delineation of epileptogenic regions during intra-operative electrocorticography. *Clin Neurophysiol*, *129*(10), 2089–2098. https://doi.org/https://doi.org/10.1016/j.clinph.2018.06.030

Whalen, C., Maclin, EL., Fabiani, M., Gratton, G. (2008). Validation of a method for coregistering scalp recording locations with 3D structural MR images. *Hum Brain Mapp*, *29*(11), 1288–1301. https://doi.org/10.1002/hbm.20465

Xiang, J., Wang, Y., Chen, Y., Liu, Y., Kotecha, R., Huo, X., et al. (2010). Noninvasive localization of epileptogenic zones with ictal high-frequency neuromagnetic signals. *J*

Neurosurg Pediatr, *5*(1), 113–122. https://doi.org/10.3171/2009.8.PEDS09345

Zelmann, R., Mari, F., Jacobs, J., Zijlmans, M., Dubeau, F., Gotman, J. (2012). A comparison between detectors of high frequency oscillations. *Clin Neurophysiol*, *123*(1), 106–116. https://doi.org/https://doi.org/10.1016/j.clinph.2011.06.006

Zijlmans, M., Jiruska, P., Zelmann, R., Leijten, FSS., Jefferys, JGR., Gotman, J. (2012). High-frequency oscillations as a new biomarker in epilepsy. *Ann Neurol*, *71*(2), 169–178. https://doi.org/10.1002/ana.22548

Figure legend

Figure 1. Case example patient 1. (A). **Left:** Magnetoencephalography (MEG) data is overlaid on their post-operative magnetic resonance image (MRI). MEG interictal epileptiform discharges (IEDs) were located in right superior temporal gyrus (STG), displayed as blue dots, and overlapping with resected area, which is indicated by red dashed line. **Right:** Example of MEG spike/IED time series. (B). **Left:** MEG data is overlaid on their post-operative MRI. High frequency oscillations (HFOs) were identified in right Heschl gyrus and STG, displayed as green dots (virtual sensor 68,69). Red dashed line indicates area of resection. **Right:** Time series and time-frequency display of an MEG HFO event. Green dashed lines indicate HFO event. (C) **Left:** Corresponding intracranial grid data from the same patient is overlaid on a reconstructed MR surface. HFOs were identified in gd14 and gd16 and the seizure onset zone (SOZ) outlined in the blue circle was accurately identified from the intracranial data (100% specificity, gd14, gd15, gd16). The Red circle indicates the location of the MEG HFOs identified in virtual sensor 68/69 which is in close proximity to the SOZ. This patient had a right temporal lobectomy and post-operative follow up revealed Engel outcome class II; histopathology revealed focal cortical dysplasia (FCD) IIA. **Right:** Time series and time-frequency display of an intracranial electroencephalography (iEEG) HFO event. Yellow dashed lines indicate HFO event.

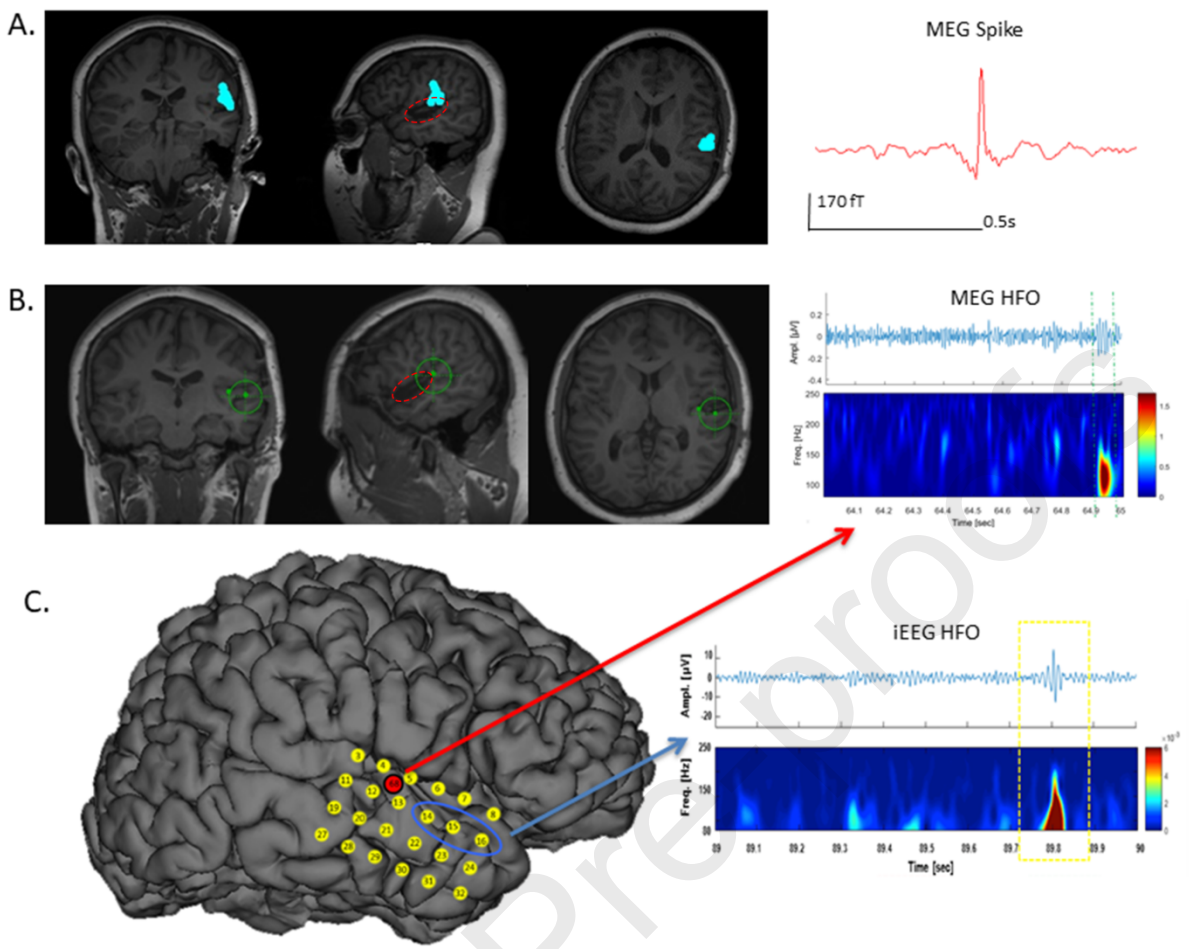

Table 1. Patient characteristics, implantation sites and details of surgery.

Pt.	Age (Yr), Gender	Age of Onset (Yr)	Implantation Type	Surgery	Pathology
1	17, F	5	R fronto-temporal grid and strips	R Temporal Lobectomy	FCD IIA
2	6, M	2.5	L fronto-parietal grid and strips	L Frontal Lesionectomy	FCD IIA
3	14, M	1	R fronto-temporal SEEG	R insular opercular, STG reseaction	FCD IB
4	9, M	2	R parietal motor-sensory grid	R Parietal Lesionectomy	DNET
5	16, M	2	L parietal grid and strip	L Parietal Lesionectomy	Meningioangiomatosis
6	16, F	10	L fronto-temporal grid and strips	L STG Resection	Gliosis

7	15, F	1	Bilateral frontal lobe SEEG	L Medial Frontal Resection	FCD IIB
8	14, F	4	R fronto-temporal SEEG	R Middle Frontal Gyrus Lesionectomy	FCD IA
9	15, M	1	L fronto-temporal SEEG	L Temporal Lobectomy & Hippocampectomy	MTS
10	7, F	1	R mesial-temporal opercular SEEG	R Temporal Lobectomy & Hippocampectomy	MTS

M=male; F=female; SEEG = stereo electroencephalography; L = left; R = right; STG = superior temporal gyrus; FCD = focal cortical dysplasia; DNET = Dysembryoplastic neuroepithelial tumor; MTS = mesial temporal sclerosis

Table 2. Results of HFO area identification in iEEG and MEG recordings, and comparison with seizure onset zone (SOZ), resection area and post-surgical outcome.

MEG and iEEG sources are listed in descending order according to the rates of HFOs.

Pt	**IEEG Implantation Type**	**iEEG Implantation Site & HFOs Rates [%]**	**iEEG Sens %**	**iEEG Spec %**	**MEG HFOs Sources & Rates [%]**	**MEG IED Dipole Sources**
1	Grid (Gd)	R Sup Temporal Gyrus: Gd14 [27], Gd16 [12]	67	100	R Heschl Gyrus [18] R Sup Temporal Gyrus [9]	R Sup Temporal Gyrus
2	Grid (Gd) & Strips	L Frontal Parietal (FP): FP3-4 [13], FP4-5 [18] L Frontal Lobe (Gd): Gd7 [15], Gd12 [11] L Sup Frontal Parietal (SFP): SFP3-4[13], SFP4-5[11]	50	89	L Precentral Gyrus [32] L Postcentral Gyrus [27]	L Precentral Gyrus
3	SEEG	R Ant Temporal (AT): AT4-5 [15], AT5-6 [25], AT6-7 [15] R Post Temporal (PT): PT4-5 [29], PT5-6 [12] R Inf Frontal (IF): IF5-6 [13]	71	88	R Sup Temporal Pole [9] R Sup Temp Gyrus [5] R Mid Temporal Pole [5] R Inf Frontal Operculum [5] R Parahippocampal Gyrus [5]	R Temporal & Parietal Lobes

4	Grid (Gd)	R Parietal Lobe: Gd12 [8], Gd13 [9], Gd15 [9], Gd22 [14], Gd23 [11], Gd28 [11], Gd31 [9]	67	79	Not Detected	No Spikes Recorded
5	Grid (Gd)	L Fronto-Parietal Lobe: Gd9 [23], Gd10 [26], Gd26 [11]	50	96	L Inf frontal operculum [9] L Paracentral Lobule [5]	No Spikes Recorded
6	Grid (Gd)	L Fronto-Temporal Lobe: Gd20 [12], Gd21 [25], Gd22 [7], Gd23 [16], Gd31 [17]	100	93	L Heschl Gyrus [7] L Rolandic Operculum [6] L Supramarginal Gyrus [5] L Sup Temporal Gyrus [5] L Sup Temporal Pole [5]	No Spikes Recorded
7	SEEG	L Ant Frontal Gyrus (F'): F'01-F'02 [10], F'05-F'06 [11] L Frontal Gyrus (E'): 0 L Primary Motor (M'): 0 R Frontal Gyrus (E): 0 R Ant Frontal Gyrus (F): F06-F07 [11]	12	96	L Mid Temporal Gyrus [6] L Inf Temporal Gyrus [6] R Postcentral Gyrus [9] R Inf Frontal Operculum [6] R Sup Parietal Gyrus [6] R Inf Parietal Gyrus [6]	L Temporal Gyrus R Temporal Gyrus R Inf Frontal Gyrus
8	SEEG	R Motor SMA (MR): MR10-11 [7], MR11-12 [5], MR5-6 [14], MR6-7 [16], MR7-8 [11], MR8-9 [13] R Ant Frontal Opercular/Insular (KR): KR1-2 [7] R Mid Frontal Opercular/Insular (ZR): 0	75	91	R Mid Temp Gyrus [12] R Sup Temp Gyrus [10] R Supramarginal Gyrus [6] R Inf Orbitofrontal Gyrus [6]	No Spikes Recorded
9	SEEG	L Sup Temporal Gyrus (TL): TL1-2 [6], TL4-5 [18] L Post Sup Temporal Gyrus (VL): VL2-3 [8], VL3-4 [11] L Ant Hippocampus (BL): BL2-3 [12]	67	92	L Sup Temporal Gyrus [11] L Sup Temporal Pole [9] L Mid Orbitofrontal Gyrus [6]	No Spikes Recorded
10	SEEG	R Ant Hippocampus (B): B1-2 [26], B2-3 [9] R Post Hippocampus (C): C1-2 [17], C2-3 [7] R Sensory Operculum/Insular (S): S5-6 [7] R Temporal basal (D): D1-2 [6]	100	95	R Sup Temporal Gyrus [6]	No Spikes Recorded

SEEG = stereo electroencephalography; Ant = anterior; Post = posterior, Inf = inferior; Sup = superior; Sens = sensitivity; Spec = specificity; L = left; R = right; G= good; M=moderate; P= poor. Engel's classification: I, free from disabling seizures (Ia, completely seizure free since surgery); II, rare disabling seizures; III, worthwhile improvement; IV, no worthwhile improvement.